applied sciences

MDPI

Article

Porous Thin-Wall Hollow Co_3O_4 Spheres for Supercapacitors with High Rate Capability

Xiao Fan [1], Yongjiao Sun [2], Per Ohlckers [1,*] and Xuyuan Chen [1,*]

[1] Department of Microsystems, University of South-Eastern Norway, Campus Vestfold, Raveien 215, 3184 Borre, Norway; xiao.fan@usn.no

[2] Micro and Nano System Research Center, College of Information and Computer, Taiyuan University of Technology, Taiyuan 030024, China; yjsun88@126.com

* Correspondence: per.ohlckers@usn.no (P.O.); xuyuan.chen@usn.no (X.C.)

Received: 25 September 2019; Accepted: 30 October 2019; Published: 2 November 2019

Abstract: In this study, a zeolitic imidazolate framework-67 (ZIF-67) was prepared as a precursor using a facile hydrothermal method. After a calcination reaction in the air, the as-prepared precursor was converted to porous thin-wall hollow Co_3O_4 with its original frame structure almost preserved. The physical and chemical characterizations of the nanomaterial were analyzed systemically. The electrochemical tests indicate that the obtained Co_3O_4 possesses large specific capacitances of 988 and 925 F/g at 1 and 20 A/g accompanying an outstanding rate capability (a 93.6% capacitance retention) and retains 96.6% of the specific capacitance, even after 6000 continuous charge/discharge cycles. These excellent properties mark the Co_3O_4 a promising electrode material for high performance supercapacitors.

Keywords: Co_3O_4; hollow structure; rate capability; supercapacitors

1. Introduction

Rapid technological development and accelerated natural resource consumption have largely increased the demand for efficient, environmentally-friendly, cost-effective, and safe energy storage devices [1–4]. In the last decade, supercapacitors—the new devices between conventional physical capacitors and lithium-ion batteries—have been extensively recognized as one of the most promising candidates for energy storage devices due to their high power density, long cycling lifespan, and fast charge/discharge process [5–11]. In general, supercapacitors can be divided into two categories according to their energy storage mechanism: One is the electric double-layer capacitor (EDLCs), which is mainly made of carbonaceous materials [12–16]; the other is the faradic redox reaction pseudocapacitor (PsCs), which usually utilizes transition metal oxides/hydroxides as electrode materials [17–21]. In particular, pseudocapacitors deliver much higher specific capacitance in comparison with electric double-layer capacitors, and receive considerable interest today [22,23].

Among various transition metal compounds, Co_3O_4 occupies a crucial position due to its superior theoretical specific capacitance (3560 F/g), nontoxicity, and low cost [24–26]. Meanwhile, the hollow structure stands out because of its novel interior geometry and surface functionality; this can possibly provide a large surface area and extra active sites, thus dramatically boosting the electrochemical properties [27,28]. To date, a great deal of efforts have been devoted to synthesizing Co_3O_4 with hollow morphologies such as hollow spheres [28], hollow nanocubes [29], and hollow cages [30]. Despite the great progress that has been made, the specific capacitance is still significantly below the theoretical value, especially at high current densities. Therefore, it is still a challenge to fully take advantage of this powerful hollow nanoscaled Co_3O_4 to achieve a large specific capacitance and a good rate capability.

In this work, we successfully prepared porous thin-wall hollow Co_3O_4 spheres from a zeolitic imidazolate framework-67 (ZIF-67) precursor through a simple and fast reaction. This nanostructure offers a large accessible surface area with numerous pathways. As a consequence, it exhibits a large specific capacitance of 988 F/g at 1 A/g with satisfactory cycling stability (96.6% retention after 6000 cycles). In particular, the specific capacitance of 925 F/g at even 20 A/g (slight decay of less than 7%) is extremely competitive among Co_3O_4-based electrode materials reported in literature. The pseudocapacitive performance manifests the great potential of the porous thin-wall hollow Co_3O_4 spheres as electrode materials for applications in supercapacitors.

2. Materials and Methods

2.1. Sample Preparation

All reagents were of analytical grade and were used as received without any further purification. First, 0.437 g of $Co(NO_3)_2{\cdot}6H_2O$ and 0.616 g of 2-methyl imidazole were briefly dissolved in respective 20 mL methanol solutions. Then, the latter solution was added dropwise into the prior one under vigorous stirring. After an ultrasonic bath for 20 min, the precipitates were collected by centrifugation and washed with methanol. Partial precipitates (0.02 g) were dispersed in a 15 mL methanol solution again. Subsequently, 0.175 g of $Co(NO_3)_2{\cdot}6H_2O$ was added into the separated solution. The resulting mixture was transferred to a Teflon-lined stainless-steel autoclave and heated at 120 °C for 1 h. The separated products were washed with methanol and dried at 60 °C. Finally, the porous thin-wall hollow Co_3O_4 spheres were obtained via heat treatment at 400 °C for 2 h.

2.2. Material Characterizations

The crystal structure of as-obtained Co_3O_4 was recorded by X-ray powder diffraction (XRD, EQUINOX 1000) with Cu–Kα_1 radiation (λ = 1.5406 Å). Scanning electron microscopy (SEM, Hitachi SU8230) with energy-dispersive X-ray (EDX) spectrum was performed for characterizations of morphology and element composition. X-ray photoelectron spectroscopy (XPS) was collected on an ESCALAB 250Xi.

2.3. Electrochemical Measurements

The Co_3O_4, acetylene black, and polyvinylidene fluoride (PVDF) with a weight ratio of 80:15:5 were dispersed in n-methyl-2-pyrrolidone (NMP) solution and ground continuously for 10 min in a mortar to form a slurry. The working electrode was prepared by pressing the slurry on nickel foam (NF). The electrochemical measurements were carried out at room temperature in a typical three-electrode system (2M KOH as the electrolyte), in which a Pt net and Ag/AgCl were used as a counter electrode and a reference electrode, respectively. A cyclic voltammogram (CV) was conducted at various scan rates and galvanostatic charge/discharge (GCD) was tested at different current densities. The specific capacitance (C, F/g) based on CV is defined as:

$$C = \frac{\int i(V)dV}{2mv\Delta V}, \tag{1}$$

and the specific capacitance based on GCD is given by:

$$C = \frac{It}{m\Delta V}, \tag{2}$$

where $\int i(V)dV$ (V·A) is the integrated area of the CV curve, and m (g), v (V/s), ΔV (V), I (A/g), and t (s) are the mass of active material, scan rate, potential window, discharge current, and discharge time [31,32]. The electrochemical impedance spectrum (EIS) was determined over a frequency range

from 100 mHz to 100 kHz with an AC perturbation of 5 mV at open circuit potential. The cycling performance was evaluated through repetitive GCD tests.

3. Results and Discussion

The morphology of as-prepared Co_3O_4 was investigated by SEM. Figure 1 presents SEM images of the precursor (Figure 1a,b) and the calcined Co_3O_4 (Figure 1c,d). Surprisingly, the Co_3O_4 effectively inherited the morphology of the precursor (negligible size contraction and few broken pieces) and exhibits uniform spherical structures. Furthermore, the magnified image (Figure 1d) shows that the spheres tend to interconnect with one another and clearly confirms the hollow nature, as well as the thin shell thickness of the Co_3O_4 from the view of a broken piece. The diameter of the spheres lies between 500 and 600 nm. In addition, the shell is assembled from numerous nanoparticles, constructing a highly porous architecture. This structure results in more active sites on the surface and easier transportation of ions, leading to better electrochemical performance.

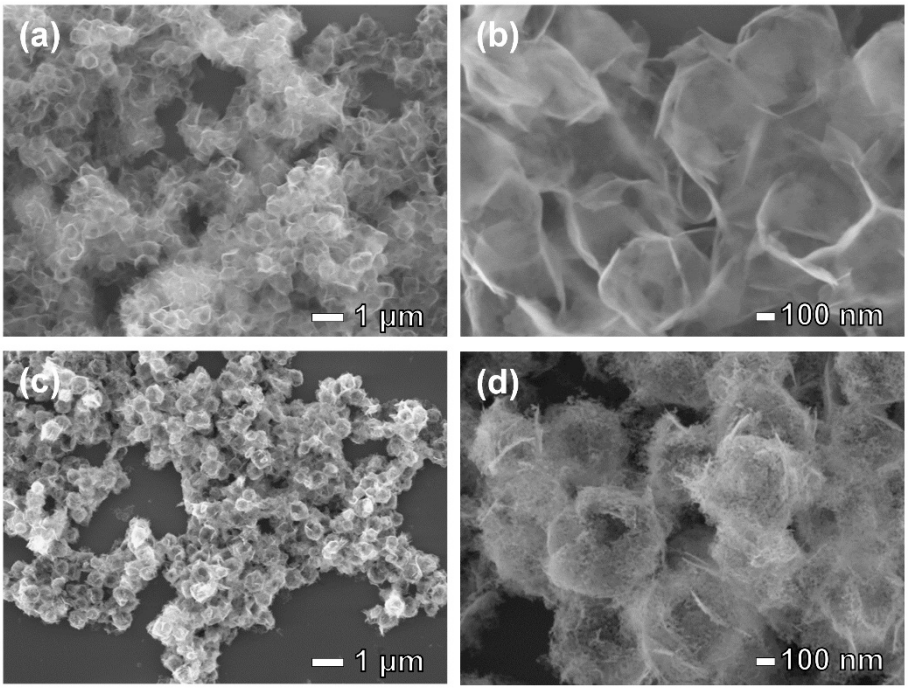

Figure 1. SEM images of (**a**) low- and (**b**) high-magnification of the precursor; (**c**) low- and (**d**) high-magnification of the calcined Co_3O_4.

The XRD patterns seen in Figure 2a, where the eight identified diffraction peaks located at 19°, 31.3, 36.9, 38.6, 44.9, 55.8, 59.5, and 65.4° are indexed to the (111), (220), (311), (222), (400), (422), (511), and (440) planes respectively, are perfectly consistent with the cubic phase of Co_3O_4 (JCPDS card No. 65-3103) [33]. The element compositions were confirmed by EDX, as depicted in Figure 2b. The peaks correspond to the elements Co and O, respectively. No other impurity element was observed. Both XRD and EDX characterizations reveal the high purity of the product.

The XPS was used to analyze the surface component and valence state of the as-obtained Co_3O_4. In the Co 2p core-level XPS spectrum seen in Figure 3a, the Co 2p was deconvoluted into two doublets. The peaks at 779.4 and 794.4 eV are related to Co^{3+}, and the peaks at 780.4 and 795.7 eV are assigned to Co^{2+} [34]. In the high-resolution XPS spectrum of O 1s seen in Figure 3b, the O 1s can be fit into three different peaks at binding energies of 529.9, 530,9, and 532 eV, which are referenced to the lattice oxygen, the OH^- species absorbed onto surface, and the multiplicity of physical and chemical absorbed water near surface, respectively [35]. This analysis of XPS further verifies the successful synthesis of the Co_3O_4.

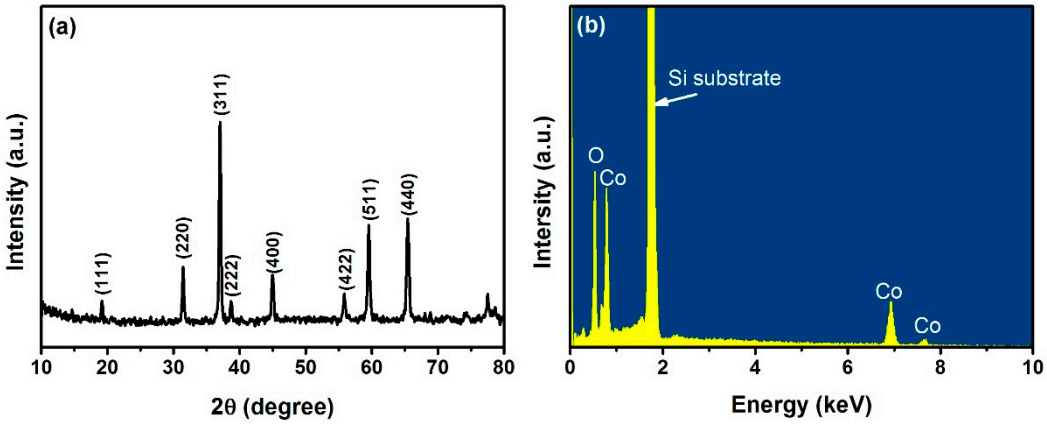

Figure 2. (**a**) XRD patterns and (**b**) energy-dispersive X-ray (EDX) spectrum of the obtained Co_3O_4.

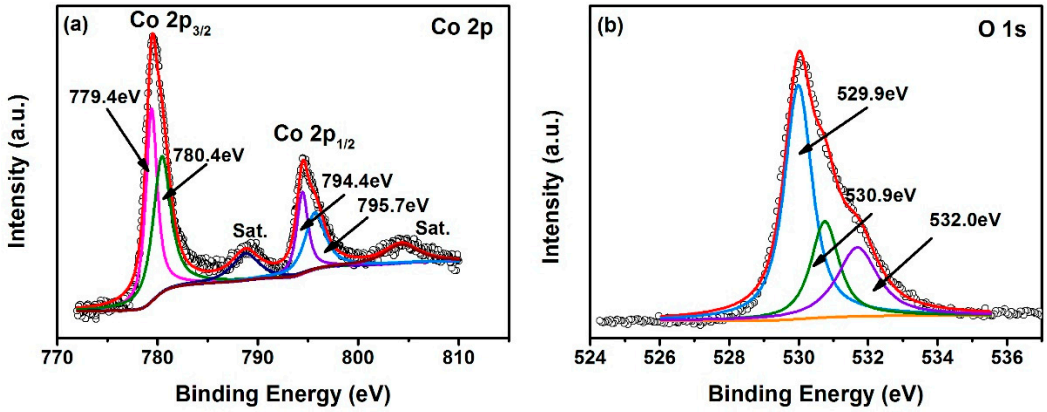

Figure 3. High-resolution X-ray photoelectron spectroscopy (XPS) scan of as-obtained Co_3O_4: (**a**) Co 2p region; (**b**) O 1s region.

The electrochemical performance of as-formed Co_3O_4 as an electrode material for supercapacitors was evaluated systematically. Figure 4a shows CV curves of the Co_3O_4 at various scan rates within a potential window of 0–0.55 V. As expected, the CV curve shape is totally different from those of electric double-layer capacitors (which have an almost rectangular shape), which reveals that the capacitance characteristics of the Co_3O_4 are those of typical pseudocapacitive capacitance. Additionally, two distinct pairs of redox peaks are visible in the CV curves. The first redox couple is ascribed to the faradic redox reaction of Co^{2+}/Co^{3+}, expressed as Equation (3) [29,30,36]:

$$Co_3O_4 + OH^- + H_2O \leftrightarrow 3CoOOH + e^-, \quad (3)$$

and the second redox couple corresponds to the conversion of Co^{3+}/Co^{4+}, expressed as Equation (4) [29,30,36]:

$$CoOOH + OH^- \leftrightarrow CoO_2 + H_2O + e^-. \quad (4)$$

When the scan rate increases from 5 to 100 mV/s, the peak current increases enormously. Furthermore, the anodic and cathodic peaks shift to higher and to lower potentials, suggesting classical pseudocapacitive behavior. The CV curve of the Co_3O_4 at 100 mV/s retains a redox shape similar to the original shape at 5 mV/s. It implies that the Co_3O_4 possesses an excellent rate capability, which is further confirmed by the calculated specific capacitances.

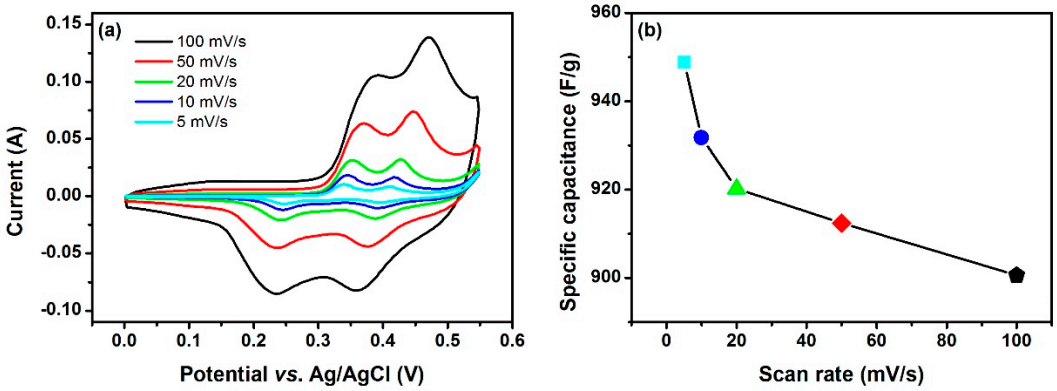

Figure 4. (**a**) Cyclic voltammogram (CV) curves and (**b**) specific capacitances of the Co_3O_4 electrode at various scan rates.

On the basis of Equation (1), the specific capacitances were determined to be 948.9, 931.8, 920.2, 912.4, and 900.6 F/g at scan rates of 5, 10, 20, 50, and 100 mV/s respectively, as shown in Figure 4b. The prominent specific capacitances most probably benefit from the porous hollow sphere nanostructure. The decrease in specific capacitances with an increasing scan rate can be understood in terms of the circuitous diffusion of OH^- ions into the Co_3O_4. At a low scan rate, both the inner and outer surface of the material can be utilized for charge storage. At a high scan rate, the diffusion of OH^- ions is more likely happen on the outer surface and only a small fraction of OH^- ions can penetrate into the inner surface [37]. Nevertheless, the inevitable decrease of specific capacitances is not drastic, which demonstrates an excellent rate capability (maintaining almost 95% capacitance from 5 to 100 mV/s). This phenomenon illustrates that the Co_3O_4 is able to act as a "reservoir" of ions [38,39] to accommodate OH^-. The reservoir can guarantee the efficient proceeding of the faradic reactions at high scan rates (or high current densities) and in turn relieves the fading of the specific capacitances. Further evidence is provided by GCD measurement.

The discharge curves of the Co_3O_4 measured at different current densities in a voltage window of 0–0.55 V are presented in Figure 5a. In comparison with the discharge curves of electric double-layer capacitors (which are almost a straight line), two evident plateaus are well displayed. These coincide with the sequential redox reactions described by Equations (3) and (4), indicating the pseudocapacitive property of the Co_3O_4. According to Equation (2), specific capacitances of 988, 960, 947.9, 939.4, and 925 F/g can be delivered at current densities of 1, 2, 5, 10, and 20 A/g respectively, as depicted by Figure 5b. Due to the relatively insufficient active material involved in redox reactions under higher current densities, the boosting of the current densities results in the fading of specific capacitances. At a low current density, the OH^- ions have adequate time to transfer at the interface between electrode and electrolyte than they do at a high current density [40]. It is worth noting that the rate performance of the Co_3O_4 is impressive (maintaining 925 F/g at 20 A/g, representing a 93.6% capacitance retention), which is significant for practical use of the material.

An EIS study is depicted in Figure 6. The first intersection point of the Nyquist plot with the real axis reflects the resistances (R_s), including the ionic resistance of the electrolyte, contact resistance at the interface of electrolyte and electrode, and intrinsic resistance of the material [39]. The Co_3O_4 modified electrode exhibits a very low R_s of 0.52 Ohms. In the high frequency region, the charge-transfer resistance (R_{ct}) and double-layer capacitance (C_{dl}) correspond to the semicircle arc. The inset of Figure 6 shows that the semicircle has a small diameter, expressing a low charge-transfer resistance and a low interfacial resistance between the current collector and electroactive material [22,41]. In the low frequency range, the slope of the plot corresponds to the diffusive resistance of OH^- ions (Warburg impedance, W) within the Co_3O_4. The plot presents an evident straight line with a slope greater than 45°, which indicates a valid electrolyte ion diffusion [30,34]. The equivalent circuit fitting the

impedance spectrum, which involves R_s, R_{ct}, C_{dl}, W, and pseudocapacitance (C_{ps}), is shown in the inset of Figure 6.

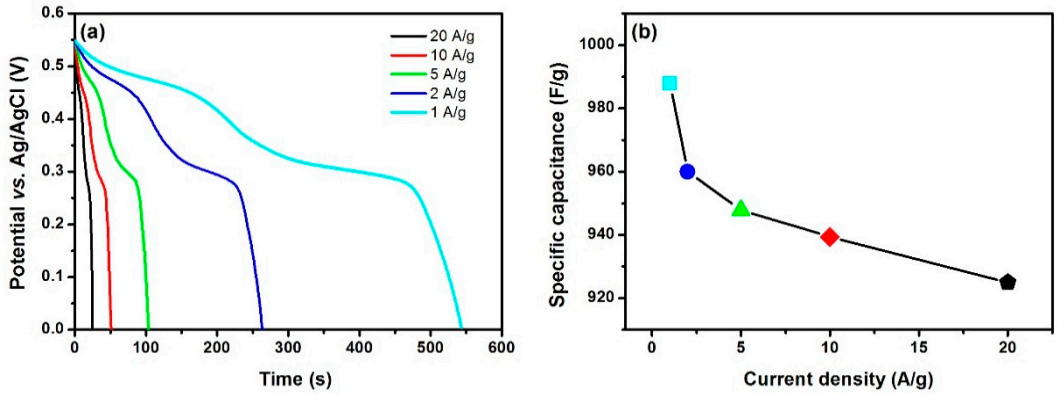

Figure 5. (**a**) Discharge curves and (**b**) specific capacitances of the Co_3O_4 electrode at different current densities.

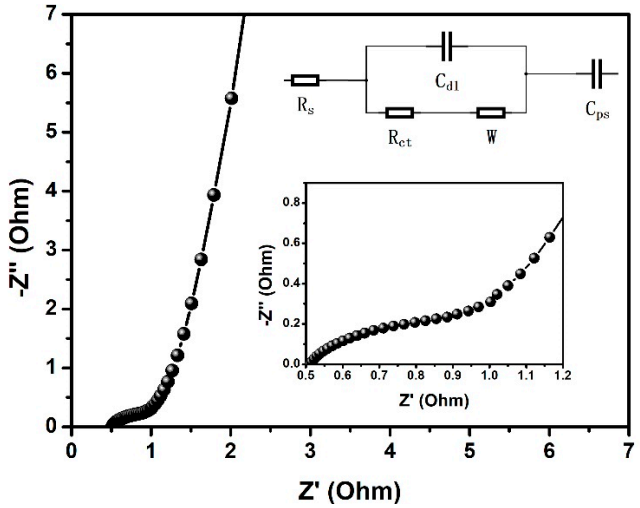

Figure 6. Electrochemical impedance spectrum (EIS) plot of the Co_3O_4 electrode over a frequency range from 100 mHz to 100 kHz. The insets show the equivalent circuit and an enlarged view of the high frequency region.

Long-term cycling stability is an important parameter required for practical application. Hence, the GCD tests were repeated for 6000 cycles at a current density of 20 A/g. As shown in Figure 7, 96.6% of the specific capacitance value is still retained. In addition, the coulombic efficiency is deduced from Equation (5) [37,39]:

$$\eta = \frac{t_d}{t_c}, \tag{5}$$

where t_d (s) and t_c (s) are, respectively, the discharge and charge times; a high efficiency exceeding 95% is achieved. This reveals that long-lasting cycling assessment does no obvious damage to the nanostructure and a feasible redox process is generated from the obtained material and verifies the remarkable electrochemical stability.

A comparison between our work and Co_3O_4-based electrode materials in current reports was made, as summarized in Table 1. Unfortunately, the high capacitive performances obtained through tremendous efforts usually accompany poor rate capability, which severely limits their wide application in high-power energy storage devices. The Co_3O_4 in this paper can meet the need of not only high specific capacitance but also excellent rate capability. In addition, the performance of the Co_3O_4 is

even better than some composites of cobalt oxides [34,42,43]. The superior electrochemical behaviors can first be explained by the stable morphology. Secondly, the large surface and inner space favors an efficient contact between active material and electrolyte, ensuring a high utilization rate of active material. Thirdly, the interconnected nanoparticles with an increased surface-to-bulk ratio offer more sites for ions to enter and, more importantly, allow facile ion diffusion at a high current density [44]. Finally, the hollow spheres are interconnected with one another, contributing to an even longer ionic diffusion channel [37].

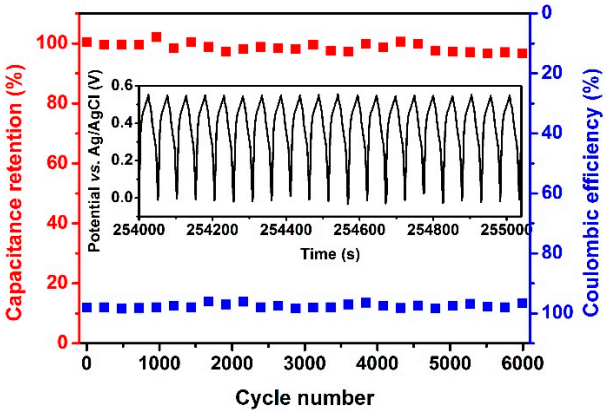

Figure 7. Cycling performance and coulombic efficiency of the Co_3O_4 electrode.

Table 1. Brief capacitance, rate, and cycling performance list of Co_3O_4-based electrode materials.

Material	Specific Capacitance	Rate Capability	Stability-Cycles	Ref.
hollow Co_3O_4 spheres	474.8 F/g at 1 A/g	79% at 10 A/g	99%-1000	[37]
hollow Co_3O_4 spheres	394.4 F/g at 2 A/g	81% at 20 A/g	92%-500	[45]
hollow Co_3O_4 spheres	342.1 F/g at 0.5 A/g	69% at 10 A/g	90%-2000	[46]
hollow Co_3O_4 nanotubes	1006 F/g at 1 A/g	51% at 10 A/g	91%-1000	[29]
hollow Co_3O_4 cages	948.9 F/g at 1 A/g	56.6% at 40 A/g	–	[30]
hollow Co_3O_4 nanotubes	404.9 F/g at 0.5 A/g	87.8% at 20 A/g	95%-2000	[38]
hollow Co_3O_4 3D-nanonet	739 F/g at 1 A/g	72% at 15 A/g	90.2%-1000	[39]
hollow Co_3O_4 flowers	210 F/g at 0.5 A/g	86% at 10 A/g	–	[46]
hollow Co_3O_4 corals	527 F/g at 1 A/g	78% at 10 A/g	99%-5000	[47]
hollow Co_3O_4 nanowires	599 F/g at 2 A/g	73% at 40 A/g	91%-7500	[48]
hollow Co_3O_4 boxes	278 F/g at 0.5 A/g	63% at 5 A/g	–	[49]
hollow Co_3O_4 dodecahedron	1100 F/g at 1.25 A/g	40% at 12.5 A/g	95.1%-6000	[50]
Co_3O_4 spheres	837.7 F/g at 1 A/g	93.6% at 10 A/g	87%-2000	[51]
Co_3O_4 spheres	261.1 F/g at 0.5 A/g	42% at 5 A/g	90.2%-2000	[52]
Co_3O_4 nanorods	739 F/g at 5 mV/s	52.5% at 100 mV/s	103%-50000	[53]
Co_3O_4 nanowires	977 F/g at 2 A/g	49.5% at 10 A/g	90%-2000	[54]
Co_3O_4 nanoflakes	450 F/g at 1 A/g	81% at 20 A/g	92%-5000	[55]
Mn doped Co_3O_4	668.4 F/g at 1 A/g	62% at 10 A/g	104%-10000	[34]
Au decorated Co_3O_4	681 F/g at 0.5 A/g	58% at 10 A/g	83.1%-13000	[42]
CoO/Co_3O_4	451 F/g at 1 A/g	68.3% at 20 A/g	108%-5000	[43]
hollow Co_3O_4 spheres	988 F/g at 1 A/g	93.6% at 20 A/g	96.6%-6000	Ours

4. Conclusions

In summary, porous thin-wall hollow Co_3O_4 spheres were successfully prepared through a simple approach and were characterized in detail. The electrochemical studies above unambiguously illuminate that the Co_3O_4 in this work shows prominent specific capacitance and cycling stability, which are attributed to its favorable structural features. Particularly, in comparison with other Co_3O_4-based electrode materials, it demonstrates an overwhelming rate capability (limited decay of 6.4% from

1 to 20 A/g), which is very critical for commercial applications. These results indicate the exciting supercapacitor application potential of our synthesized material. Moreover, the relationship between the structure and properties is worth investigating in depth in the future.

Author Contributions: X.F. investigated the research, performed the characterizations and analyzed the data; X.F. and Y.S. contributed equally to conduct the experiments and to write the manuscript; P.O. provided the critical feedback and designed the structure of the manuscript; P.O. and X.C. both equally supervised the experiments and refined the manuscript.

Funding: This research was funded by the Norwegian PhD Network on Nanotechnology for Microsystems, which is sponsored by the Research Council of Norway, Division for Science, under contract no. 221860/F60. X.F. was funded by China Scholarship Council.

Acknowledgments: Fruitful discussions with Einar Halvorsen and Pai Lu are acknowledged.

Conflicts of Interest: The authors declare no conflict of interest.

References

1. Hui, K.N.; San Hui, K.; Tang, Z.; Jadhav, V.V.; Xia, Q.X. Hierarchical chestnut-like $MnCo_2O_4$ nanoneedles grown on nickel foam as binder-free electrode for high energy density asymmetric supercapacitors. *J. Power Sources* **2016**, *330*, 195–203. [CrossRef]
2. Cui, L.; Huang, L.; Ji, M.; Wang, Y.; Shi, H.; Zuo, Y.; Kang, S. High-performance $MgCo_2O_4$ nanocone arrays grown on three-dimensional nickel foams: Preparation and application as binder-free electrode for pseudo-supercapacitor. *J. Power Sources* **2016**, *333*, 118–124. [CrossRef]
3. Tang, Z.; Tang, C.H.; Gong, H. A high energy density asymmetric supercapacitor from nano-architectured $Ni(OH)_2$/Carbon nanotube electrodes. *Adv. Funct. Mater.* **2012**, *22*, 1272–1278. [CrossRef]
4. Roy, A.; Jadhav, H.S.; Thorat, G.M.; Seo, J.G. Electrochemical growth of $Co(OH)_2$ nanoflakes on Ni foam for methanol electro-oxidation. *New J. Chem.* **2017**, *41*, 9546–9553. [CrossRef]
5. Wang, C.; Zhou, E.; He, W.; Deng, X.; Huang, J.; Ding, M.; Wei, X.; Liu, X.; Xu, X. $NiCo_2O_4$-based supercapacitor nanomaterials. *Nanomaterials* **2017**, *7*, 41. [CrossRef] [PubMed]
6. Simon, P.; Gogotsi, Y.; Dunn, B. Where do batteries end and supercapacitors begin? *Science* **2014**, *343*, 1210–1211. [CrossRef]
7. Conway, B.E. Transition from "supercapacitor" to "battery" behavior in electrochemical energy storage. *J. Electrochem. Soc.* **1991**, *138*, 1539–1548. [CrossRef]
8. González, A.; Goikolea, E.; Barrena, J.A.; Mysyk, R. Review on supercapacitors: Technologies and materials. *Renew. Sustain. Energy Rev.* **2016**, *58*, 1189–1206. [CrossRef]
9. Vangari, M.; Pryor, T.; Jiang, L. Supercapacitors: Review of materials and fabrication methods. *J. Energy Eng.* **2012**, *139*, 72–79. [CrossRef]
10. Miller, J.R.; Simon, P. Electrochemical capacitors for energy management. *Science* **2008**, *321*, 651–652. [CrossRef]
11. Kötz, R.; Carlen, M. Principles and applications of electrochemical capacitors. *Electrochim. Acta* **2000**, *45*, 2483–2498. [CrossRef]
12. Lu, P.; Müller, L.; Hoffmann, M.; Chen, X. Taper silicon nano-scaffold regulated compact integration of 1D nanocarbons for improved on-chip supercapacitor. *Nano Energy* **2017**, *41*, 618–625. [CrossRef]
13. Zhang, L.L.; Zhao, X.S. Carbon-based materials as supercapacitor electrodes. *Chem. Soc. Rev.* **2009**, *38*, 2520–2531. [CrossRef] [PubMed]
14. Wang, Y.; Shi, Z.; Huang, Y.; Ma, Y.; Wang, C.; Chen, M.; Chen, Y. Supercapacitor devices based on graphene materials. *J. Phys. Chem. C* **2009**, *113*, 13103–13107. [CrossRef]
15. Zhang, L.L.; Zhou, R.; Zhao, X.S. Graphene-based materials as supercapacitor electrodes. *J. Mater. Chem.* **2010**, *20*, 5983–5992. [CrossRef]
16. Pan, H.; Li, J.; Feng, Y. Carbon nanotubes for supercapacitor. *Nanoscale Res. Lett.* **2010**, *5*, 654. [CrossRef]
17. Yu, Z.; Tetard, L.; Zhai, L.; Thomas, J. Supercapacitor electrode materials: Nanostructures from 0 to 3 dimensions. *Energy Environ. Sci.* **2015**, *8*, 702–730. [CrossRef]
18. Sk, M.M.; Yue, C.Y.; Ghosh, K.; Jena, R.K. Review on advances in porous nanostructured nickel oxides and their composite electrodes for high-performance supercapacitors. *J. Power Sources* **2016**, *308*, 121–140. [CrossRef]

19. Chen, H.; Hu, L.; Chen, M.; Yan, Y.; Wu, L. Nickel–cobalt layered double hydroxide nanosheets for high-performance supercapacitor electrode materials. *Adv. Funct. Mater.* **2014**, *24*, 934–942. [CrossRef]
20. Zhi, M.; Xiang, C.; Li, J.; Li, M.; Wu, N. Nanostructured carbon–metal oxide composite electrodes for supercapacitors: A review. *Nanoscale* **2013**, *5*, 72–88. [CrossRef]
21. Lin, L.; Tang, S.; Zhao, S.; Peng, X.; Hu, N. Hierarchical three-dimensional $FeCo_2O_4$@MnO_2 core-shell nanosheet arrays on nickel foam for high-performance supercapacitor. *Electrochim. Acta* **2017**, *228*, 175–182. [CrossRef]
22. Qiu, M.; Sun, P.; Shen, L.; Wang, K.; Song, S.; Yu, X.; Tan, S.; Zhao, C.; Mai, W. WO_3 nanoflowers with excellent pseudo-capacitive performance and the capacitance contribution analysis. *J. Mater. Chem. A* **2016**, *4*, 7266–7273. [CrossRef]
23. Liu, J.; Jiang, J.; Cheng, C.; Li, H.; Zhang, J.; Gong, H.; Fan, H.J. Co_3O_4 nanowire@MnO_2 ultrathin nanosheet core/shell arrays: A new class of high-performance pseudocapacitive materials. *Adv. Mater.* **2011**, *23*, 2076–2081. [CrossRef] [PubMed]
24. Yuan, C.; Yang, L.; Hou, L.; Li, J.; Sun, Y.; Zhang, X.; Shen, L.; Lu, X.; Xiong, S.; Lou, X.W. Flexible hybrid paper made of monolayer Co_3O_4 microsphere arrays on rGO/CNTs and their application in electrochemical capacitors. *Adv. Funct. Mater.* **2012**, *22*, 2560–2566. [CrossRef]
25. Li, Z.Y.; Bui, P.T.; Kwak, D.H.; Akhtar, M.S.; Yang, O.B. Enhanced electrochemical activity of low temperature solution process synthesized Co_3O_4 nanoparticles for pseudo-supercapacitors applications. *Ceram. Int.* **2016**, *42*, 1879–1885. [CrossRef]
26. Rakhi, R.B.; Chen, W.; Cha, D.; Alshareef, H.N. Substrate dependent self-organization of mesoporous cobalt oxide nanowires with remarkable pseudocapacitance. *Nano Lett.* **2012**, *12*, 2559–2567. [CrossRef]
27. He, T.; Chen, D.; Jiao, X.; Xu, Y.; Gu, Y. Surfactant-assisted solvothermal synthesis of Co_3O_4 hollow spheres with oriented-aggregation nanostructures and tunable particle size. *Langmuir* **2004**, *20*, 8404–8408. [CrossRef]
28. Xia, X.H.; Tu, J.P.; Wang, X.L.; Gu, C.D.; Zhao, X.B. Mesoporous Co_3O_4 monolayer hollow-sphere array as electrochemical pseudocapacitor material. *Chem. Commun.* **2011**, *47*, 5786–5788. [CrossRef]
29. Yao, M.; Hu, Z.; Xu, Z.; Liu, Y. Template synthesis of 1D hierarchical hollow Co_3O_4 nanotubes as high performance supercapacitor materials. *J. Alloys Compd.* **2015**, *644*, 721–728. [CrossRef]
30. Zhou, X.; Shen, X.; Xia, Z.; Zhang, Z.; Li, J.; Ma, Y.; Qu, Y. Hollow fluffy Co_3O_4 cages as efficient electroactive materials for supercapacitors and oxygen evolution reaction. *ACS Appl. Mater. Interfaces* **2015**, *7*, 20322–20331. [CrossRef]
31. Lu, P.; Ohlckers, P.; Müller, L.; Leopold, S.; Hoffmann, M.; Grigoras, K.; Ahopelto, J.; Prunnila, M.; Chen, X. Nano fabricated silicon nanorod array with titanium nitride coating for on-chip supercapacitors. *Electrochem. Commun.* **2016**, *70*, 51–55. [CrossRef]
32. Lu, P.; Halvorsen, E.; Ohlckers, P.; Müller, L.; Leopold, S.; Hoffmann, M.; Grigoras, K.; Ahopelto, J.; Prunnila, M.; Chen, X. Ternary composite Si/TiN/MnO_2 taper nanorod array for on-chip supercapacitor. *Electrochim. Acta* **2017**, *248*, 397–408. [CrossRef]
33. Li, W.Y.; Xu, L.N.; Chen, J. Co_3O_4 nanomaterials in lithium-ion batteries and gas sensors. *Adv. Funct. Mater.* **2005**, *15*, 851–857. [CrossRef]
34. Li, G.; Chen, M.; Ouyang, Y.; Yao, D.; Lu, L.; Wang, L.; Xia, X.; Lei, W.; Chen, S.M.; Hao, Q. Manganese doped Co_3O_4 mesoporous nanoneedle array for long cycle-stable supercapacitors. *Appl. Surf. Sci.* **2019**, *469*, 941–950. [CrossRef]
35. Wu, H.B.; Pang, H.; Lou, X.W.D. Facile synthesis of mesoporous $Ni_{0.3}Co_{2.7}O_4$ hierarchical structures for high-performance supercapacitors. *Energy Environ. Sci.* **2013**, *6*, 3619–3626. [CrossRef]
36. Wang, D.; Wang, Q.; Wang, T. Morphology-controllable synthesis of cobalt oxalates and their conversion to mesoporous Co_3O_4 nanostructures for application in supercapacitors. *Inorg. Chem.* **2011**, *50*, 6482–6492. [CrossRef]
37. Du, H.; Jiao, L.; Wang, Q.; Yang, J.; Guo, L.; Si, Y.; Wang, Y.; Yuan, H. Facile carbonaceous microsphere templated synthesis of Co_3O_4 hollow spheres and their electrochemical performance in supercapacitors. *Nano Res.* **2013**, *6*, 87–98. [CrossRef]
38. Zhao, C.; Huang, B.; Fu, W.; Chen, J.; Zhou, J.; Xie, E. Fabrication of porous nanosheet-based Co_3O_4 hollow nanocubes for electrochemical capacitors with high rate capability. *Electrochim. Acta* **2015**, *178*, 555–563. [CrossRef]

39. Wang, Y.; Lei, Y.; Li, J.; Gu, L.; Yuan, H.; Xiao, D. Synthesis of 3D-nanonet hollow structured Co_3O_4 for high capacity supercapacitor. *ACS Appl. Mater. Interfaces* **2014**, *6*, 6739–6747. [CrossRef]
40. Kumar, R.D.; Andou, Y.; Karuppuchamy, S. Microwave-assisted synthesis of Zn–WO_3 and $ZnWO_4$ for pseudocapacitor applications. *J. Phys. Chem. Solids* **2016**, *92*, 94–99. [CrossRef]
41. Ede, S.R.; Ramadoss, A.; Nithiyanantham, U.; Anantharaj, S.; Kundu, S. Bio-molecule assisted aggregation of $ZnWO_4$ nanoparticles (NPs) into chain-like assemblies: Material for high performance supercapacitor and as catalyst for benzyl alcohol oxidation. *Inorg. Chem.* **2015**, *54*, 3851–3863. [CrossRef] [PubMed]
42. Tan, Y.; Liu, Y.; Kong, L.; Kang, L.; Ran, F. Supercapacitor electrode of nano-Co_3O_4 decorated with gold nanoparticles via in-situ reduction method. *J. Power Sources* **2017**, *363*, 1–8. [CrossRef]
43. Pang, M.; Long, G.; Jiang, S.; Ji, Y.; Han, W.; Wang, B.; Liu, X.; Xi, Y.; Wang, D.; Xu, F. Ethanol-assisted solvothermal synthesis of porous nanostructured cobalt oxides (CoO/Co_3O_4) for high-performance supercapacitors. *Chem. Eng. J.* **2015**, *280*, 377–384. [CrossRef]
44. Yang, G.W.; Xu, C.L.; Li, H.L. Electrodeposited nickel hydroxide on nickel foam with ultrahigh capacitance. *Chem. Commun.* **2008**, 6537–6539. [CrossRef] [PubMed]
45. Wang, Y.; Pan, A.; Zhu, Q.; Nie, Z.; Zhang, Y.; Tang, Y.; Liang, S.; Cao, G. Facile synthesis of nanorod-assembled multi-shelled Co_3O_4 hollow microspheres for high-performance supercapacitors. *J. Power Sources* **2014**, *272*, 107–112. [CrossRef]
46. Zhu, Z.; Han, C.; Li, T.T.; Hu, Y.; Qian, J.; Huang, S. MOF-templated syntheses of porous Co_3O_4 hollow spheres and micro-flowers for enhanced performance in supercapacitors. *CrystEngComm* **2018**, *20*, 3812–3816. [CrossRef]
47. Wang, X.; Zhang, N.; Chen, X.; Liu, J.; Lu, F.; Chen, L.; Shao, G. Facile precursor conversion synthesis of hollow coral-shaped Co_3O_4 nanostructures for high-performance supercapacitors. *Colloids Surf. A* **2019**, *570*, 63–72. [CrossRef]
48. Xia, X.H.; Tu, J.P.; Mai, Y.J.; Wang, X.L.; Gu, C.D.; Zhao, X.B. Self-supported hydrothermal synthesized hollow Co_3O_4 nanowire arrays with high supercapacitor capacitance. *J. Mater. Chem.* **2011**, *21*, 9319–9325. [CrossRef]
49. Du, W.; Liu, R.; Jiang, Y.; Lu, Q.; Fan, Y.; Gao, F. Facile synthesis of hollow Co_3O_4 boxes for high capacity supercapacitor. *J. Power Sources* **2013**, *227*, 101–105. [CrossRef]
50. Zhang, Y.Z.; Wang, Y.; Xie, Y.L.; Cheng, T.; Lai, W.Y.; Pang, H.; Huang, W. Porous hollow Co_3O_4 with rhombic dodecahedral structures for high-performance supercapacitors. *Nanoscale* **2014**, *6*, 14354–14359. [CrossRef]
51. Liu, Z.; Zhou, W.; Wang, S.; Du, W.; Zhang, H.; Ding, C.; Du, Y.; Zhu, L. Facile synthesis of homogeneous core-shell Co_3O_4 mesoporous nanospheres as high performance electrode materials for supercapacitor. *J. Alloys Compd.* **2019**, *774*, 137–144. [CrossRef]
52. Guo, D.; Song, X.; Li, F.; Tan, L.; Ma, H.; Zhang, L.; Zhao, Y. Oriented synthesis of Co_3O_4 core-shell microspheres for high-performance asymmetric supercapacitor. *Colloids Surf. A* **2018**, *546*, 1–8. [CrossRef]
53. Cheng, G.; Kou, T.; Zhang, J.; Si, C.; Gao, H.; Zhang, Z. O_2^{2-}/O^- functionalized oxygen-deficient Co_3O_4 nanorods as high performance supercapacitor electrodes and electrocatalysts towards water splitting. *Nano Energy* **2017**, *38*, 155–166. [CrossRef]
54. Wang, Y.; Zhou, T.; Jiang, K.; Da, P.; Peng, Z.; Tang, J.; Kong, B.; Cai, W.B.; Yang, Z.; Zheng, G. Reduced mesoporous Co_3O_4 nanowires as efficient water oxidation electrocatalysts and supercapacitor electrodes. *Adv. Energy Mater.* **2014**, *4*, 1400696. [CrossRef]
55. Xiao, A.; Zhou, S.; Zuo, C.; Zhuan, Y.; Ding, X. Controllable synthesis of mesoporous Co_3O_4 nanoflake array and its application for supercapacitor. *Mater. Res. Bull.* **2014**, *60*, 674–678. [CrossRef]

© 2019 by the authors. Licensee MDPI, Basel, Switzerland. This article is an open access article distributed under the terms and conditions of the Creative Commons Attribution (CC BY) license (http://creativecommons.org/licenses/by/4.0/).